LEX LOCALIS-JOURNAL OF LOCAL SELF-GOVERNMENT
ISSN:1581-5374 E-ISSN:1855-363X
VOL. 23, NO. S6(2025)

INTEGRATING INTELLIGENT VISUALIZATION TO ELEVATE DIAGNOSTIC PERFORMANCE IN MEDICAL IMAGING

Muhammad Ahsan[1*], Robertas Damaševičius[1]

[1]Department of Applied Informatics, Faculty of Informatics, Vytautas Magnus University, Kaunas, Lithuania

ahsan1826@gmail.com[1*]
robertas.damasevicius@gmail.com[1]

Corresponding Author: ahsan1826@gmail.com[1]

Abstract— *Contagious and non-contagious illnesses represent a major contributor to global death rates, with their varied and complex manifestations often hindering accurate evaluation and classification of disease severity. Different geographic regions face unique obstacles in addressing these health issues. This research employs four advanced AI-powered decision support frameworks to enhance diagnostic accuracy through medical imaging. Initially, a decision support method based on entropy has been utilized, wherein entropy is calculated either at the pixel or regional level from medical images (like MRI or CT scans) to pinpoint zones of diagnostic uncertainty. Secondly, a similarity-based diagnostic model is utilized to determine disease presence by analyzing the input imagery. Thirdly, a decision-making model incorporating the TOPSIS (Technique for Order Preference by Similarity to Ideal Solution) method, integrated with AI algorithms, is employed to accurately classify the specific disease type, utilizing images from diverse imaging techniques. Fourth, an AHP (Analytic Hierarchy Process) framework is used to support diagnostic decisions through multi-criteria analysis, aiding in selecting the most suitable diagnosis. All computational processes and algorithms are executed in Python. Hypothetical datasets are used to demonstrate the implementation of these models in a medical diagnostic context. Visual aids are incorporated to enhance clarity and emphasize the significance and impact of the results.*

Keywords— *Artificial Intelligence, Decision support system, Medical imaging, Multi-criteria analysis*

Introduction

Throughout the previous ten years, there has been a significant escalation in the evolution of machine intelligence, especially within the discipline of profound neural computation [1,2]. Traditionally, deep neural architectures have fundamentally revolutionized the manner in which automated systems identify structures, render judgments, and assimilate information, achieving this at unparalleled velocities. These developments have facilitated the mechanization of numerous visual recognition operations [3]. Visual computing encompasses a collection of methodologies that empower digital entities to interpret and evaluate information derived from the tangible environment in the form of imagery and video streams. This progression is predominantly attributed to the implementation of complex layered network classifiers engineered to decode and categorize graphical stimuli responsibilities that formerly demanded considerable human proficiency. However, forecasting the efficacy of these architectures remains intricate and is not universally applicable. The benchmarks employed to gauge the effectiveness of deep computational models fluctuate considerably depending on the particular niche of visual interpretation and the specific objective of the framework [4,5]. This inconsistency becomes even more pronounced in narrowly defined fields like Clinical Imaging Partitioning (CIP), a pivotal scholarly domain dedicated to the recognition and demarcation of critical components within diagnostic scans. These focal areas termed as Zones of Clinical Significance (ZCSs) are essential for health evaluation and curative strategy formulation. Achieving these goals using scanning techniques such as Magnetic Resonance Imaging (MRI), Computed Tomography (CT), or radiographic imaging necessitates meticulous partitioning to diagnose illnesses, monitor pathological progression, and devise suitable therapeutic pathways. The intricacy of CIP surpasses simple image features like pixel density and structural complexity; it also encompasses vital medical decision-making processes [6]. In opposition to standard vision computing scenarios where mistakes may lead to negligible setbacks errors in

clinical imaging partitioning can result in substantial consequences like inaccurate diagnoses or unsuitable treatments, thus directly influencing patient outcomes. Hence, neural-based models utilized for CIP must be meticulously validated with assessment mechanisms tailored to their precision in isolating and outlining essential medical regions. The proliferation of intelligent computing and neural processing has notably advanced this sector, expediting the automation of challenging visual interpretation challenges. In the realm of CIP [7,8], such innovations are foundational to the autonomous extraction and annotation of clinical ZCSs, such as anatomical structures or disease markers like neoplasms. Nonetheless, appraising the effectiveness of these methodologies is seldom straightforward. The scrutiny procedures must be credible, resilient, and sufficiently rigorous for integration into healthcare environments. At present, medical experts especially diagnostic radiologists and histopathologists are beginning to recognize the revolutionary capability of deep neural-based CIP methodologies. When deployed as autonomous diagnostic utilities, these systems can greatly facilitate operations including anomaly detection, therapy planning, risk analysis, and minimizing image interpretation duration [9,10]. For instance, within radiological practice, deep neural tools can be instructed to partition and emphasize ZCSs in imaging studies like tumors or anomalies in CT and MRI scans, thereby assisting radiologists in quicker and more precise clinical evaluations. Similarly, in histopathological workflows, such models support accurate tissue categorization, thereby aiding pathologists in making critical assessments. The assimilation of these systems into routine clinical procedures boosts diagnostic fidelity and reduces the time expended on visual data analysis, allowing specialists to dedicate their efforts to detailed investigations. Since CIP methodologies directly influence vital healthcare decisions, confirming their evaluation is both exact and consistent is of utmost importance [11]. A system that performs exceptionally well under experimental conditions might yield suboptimal outcomes in practical medical applications, where variability and consequence levels are substantially elevated. Consequently, it is essential that these systems experience comprehensive verification and validation prior to real-world integration [12]. This involves the selection of performance indicators that accurately represent the model's competence across heterogeneous patient cohorts, diagnostic instruments, and noisy clinical environments. Alarmingly, an emerging issue highlights that certain scholars selectively report favorable performance indicators, sometimes approaching flawless results, while disregarding or omitting metrics that more truthfully reveal system limitations. These habits subvert the objectivity of performance assessment and can deceive clinical adopters. There are high-performing models on cleaned data, and scientists may emphasize trivial objectives or metrics that elevate performance artificially, excluding those that unveil algorithmic failure. This can be especially harmful to practitioners grounded in these models for life-critical medical choices. Though neural computation-based CIP models [13,14] hold great potential in the area of radiology, pathology, and allied medical sciences, it is important that they are tested in an open manner to establish trustworthiness as well as functional safety. Four state-of-the-art AI-driven analytical support systems have been incorporated in this work to enhance diagnostic accuracy using clinical imaging. There is first an uncertainty-based approach in which entropy is calculated at the clinical image level (MRI or CT) either at voxel or segmented area level to detect areas with uncertain diagnostic interpretation. There is secondly a similarity-based model for analysis that detects the presence of pathologies by analyzing the provided imaging material. Thirdly, to efficiently categorize disease variants among different imaging types, a decision-support mechanism based on the Technique for Order Preference by Similarity to Ideal Solution (TOPSIS) and integrated with smart algorithms is utilized. Lastly, the Analytic Hierarchy Process (AHP) is utilized for multi-parameter analysis, which assists in selecting the most suitable diagnostic inference. All the computational procedures are coded using the Python computer language, and example data sets are provided to demonstrate the application of the models in practice diagnostics. Visual plots are also presented to facilitate understanding and

demonstrate relevance and implications of results.

Related Works

This section gives a broad overview of prevalent artificial intelligence and neural network methods applied in healthcare image segmentation. It tries to give a detailed description of paradigms shifting, from the conventional AI classifiers to the latest developments in neural architectures that support automation of medical image interpretation. Importantly, this section mentions common problems such as class imbalance, less model flexibility, and excessive computation cost, all of which hinder the performance of the aforementioned. Through the thorough analysis of the inherent defects of the hitherto used methods, this section offers a platform for constructing stronger architectures with potential uses in clinic. Ding et al. [16] introduced the FTransCNN model, a fusion schema that merges convolutional neural processes (CNNs) and transformer modules into one, acquiring the strengths of both using a fuzzy logic structure. In this framework, CNN and transformer are concurrent attribute miners: the transformer is responsible for global attribute representations using channel-based attention, and the CNN is responsible for local patterns using spatial-based attention. Although this architecture enables thorough macro and micro feature integration, its two-way split nature and imprecise integration mechanism result in high processing overhead, which might confine its usage in low-resource real-time systems. Kaushal et al. [17] stressed the importance of formulating an efficient segmentation schedule with deep networks to enable detection of significant anatomy areas towards rapid partitioning. To this end, they proposed an integrated approach that combines the discriminative power of traditional CNNs with the segmentation power of SI algorithms. Their system includes modules like FCM, K-means clustering, and PSO-based optimizations along with CNNs, all aimed at improving segmentation accuracy and execution time. Through effectively integrating legacy clustering with state-of-the-art AI building blocks, the mass use of many unique algorithms introduces complexity that can undo adaptability and scalability in actual-world scenarios. To this end, they proposed an integrated approach that combines the discriminative power of traditional CNNs with the segmentation power of SI algorithms. Their system includes modules like FCM, K-means clustering, and PSO-based optimizations along with CNNs, all aimed at improving segmentation accuracy and execution time. Through effectively integrating legacy clustering with state-of-the-art AI building blocks, the mass use of many unique algorithms introduces complexity that can undo adaptability and scalability in actual-world scenarios.Narayan et al. [18] examined the essential contribution of anatomical delineation in improving multiple functionalities of medical imaging, encompassing diagnostic analytics, surgical strategizing, and intraoperative navigation. Their assessment reviews both the evolution and the state-of-the-art frameworks in medical imaging segmentation, tracing advancements across successive technological phases. Nonetheless, a conceivable drawback of their survey is its broad scope, which may trade off detailed examination of particular segmentation intricacies and techniques. Chin et al. [19] proposed the Fuzzy DBNet, an architecture combining a dual-butterfly configuration with a Fuzzy Atrous Spatial Pyramid Pooling (ASPP) module to refine segmentation performance in multi-angle image datasets. Evaluations on varied databases, such as multi-class pill images and thoracic radiographs, yielded Dice similarity coefficients of 95.05\% and 97.05\%, respectively, indicating robust partitioning capabilities. Still, the reliance on parallel data pipelines considerably escalates system complexity and operational demands. Shi et al. [20] unveiled a segmentation strategy utilizing a multichannel convolutional structure integrated with a fuzzy dynamic contour model. The initial step applies the superpixel-based SLIC algorithm to divide and annotate medical imagery into compact zones. These zones then serve as training data for the CNN to enhance the delineation of organ peripheries. Further refinement is achieved through fuzzy contour modeling, initiated from the superpixel outputs. Although this amalgamated method effectively unites

CNNs with fuzzy paradigms to elevate segmentation performance, its dependence on initial superpixel demarcation may propagate foundational inaccuracies into the conclusive results. Nagaraja et al. [21] pursued the augmentation of diagnostic precision for internal organs and correlated conditions, such as cerebrovascular incidents, by presenting an innovative angle using multimodal diagnostic imaging. Their technique employs an image fusion construct predicated on a freshly formulated hybrid meta-heuristic protocol. The fusion commences with a W-FDCuT transformation, decomposing visuals into high and low-frequency segments, thereby enabling superior assimilation of information from various imaging sources to reinforce system reliability. Ahammed et al. [22] developed an automated hair removal methodology utilizing morphological operations specifically the Black-Hat technique alongside an inpainting mechanism for processing dermatological lesion imagery. To diminish distortions and visual smudges, a Gaussian smoothing filter is applied, succeeded by automatic GrabCut segmentation to delineate pathological areas. Latent attributes within skin images are retrieved via the Gray Level Co-occurrence Matrix (GLCM) coupled with a range of statistical features, improving the analysis and classification of dermatological data.

Definition 1:Let $X = \{\alpha_j : j = 1, \ldots, n\}$ be the universe of discourse with attributes $\{\varepsilon i\}^m i=1$ and corresponding value sets $\{\delta i\}^m_{i=1}$. A Neutrosophic Hypersoft Set (NHSS) ϒA is defined by the mapping $H : \Pi^m_{i=1}\, \delta_i \rightarrow \wp(X)$ and consists of ordered triples $\upsilon A(\varepsilon i) = \{(\alpha, T_a(\alpha), I_a(\alpha), F_a(\alpha)) : \alpha \in X\}$, where $T_a(\alpha), I_a(\alpha), F_a(\alpha) \in [0,1]$ represent truth, indeterminacy, and falsity membership degrees respectively, satisfying $0 \leq T_a(\alpha)+I_a(\alpha)+F_a(\alpha) \leq 3$ for all $\alpha \in X$ [1].

Definition 2: Let Υ_A and Ψ_B be two NHSS defined on the same universe X and attribute sets. The Hamming distance between these two sets is given by: $d^s_{NHSS}(\Upsilon_A,\Psi_B)=1/3m\Sigma^m i=1\Sigma^n_{j=1}(|T_A(\varepsilon_i)(\alpha_j)-T_B(\varepsilon_i)(\alpha_j)|+|I_A(\varepsilon_i)(\alpha_j)-I_B(\varepsilon_i)(\alpha_j)|+|F_A(\varepsilon_i)(\alpha_j)-F_B(\varepsilon_i)(\alpha_j)|$). This formula represents the average sum of absolute differences between the truth, indeterminacy, and falsity degrees for all elements and all attributes [1].

Definition 3: Define Υ_A and Ψ_B and their Similarity Measure (SM) via HD for NHSS over a set U:$S'_{IFHSS}(\Upsilon_A,\Psi_B) =1/1+d^s_{IFHSS}(\Gamma_A,\Lambda_B)$ [1].

Application I

In the evolving landscape of medical diagnostics, a new methodology has been developed to enhance diagnostic accuracy and provide deeper clinical insights, particularly in brain imaging. This research introduces a novel application of Neutrosophic Hypersoft Set (NHSS) entropy to identify uncertain regions within grayscale medical images such as MRI or CT scans. The starting point of our study involved collecting real patient image from the Kaggle platform, a widely recognized repository of medical image datasets. These images, typically in standard grayscale format, were first transformed into the NHSS domain a three-valued logical framework that decomposes each pixel into components of truth (T), indeterminacy (I), and falsity (F). In this representation, the truth component is directly based on the pixel intensity, which often corresponds to the likelihood of pathological structures such as tumors. The indeterminacy is computed by local variance or standard deviation within the neighborhood window and is blur or diagnostic fuzziness level. The falsity is found as a complement to truth, i.e., absence or negation of the perceived feature. Then, the NHSS entropy for each pixel is computed using a proprietary algorithm (Algorithm I). This measure of entropy quantifies classification uncertainty by adding up the information in the T, I, and F values. Refer to Fig. 1 for more. High entropy at a pixel would suggest that the pixel is surrounded by contradictory or uncertain information that usually happens around tumor boundaries or overlapping tissue intensity regions. Low entropy would suggest clearer, certain regions. The resulting entropy map of this pixel-level analysis is then graphed as a heatmap where the light regions indicate the uncertain or diagnostically indeterminate areas of the image. As additional boost to clinical utility, the same entropy map is thresholded to generate a binary mask. Divided as output, the same in reality guides the

radiologist to regions of uncertainty and facilitates wiser, better-informed diagnosis. The step, apart from upgrading ultimate end picture quality to be made available for medical interpretation, introduces into the procedure the glaringly absent medical doubt quantification mode of medicine greatly missing even from current practice state. In clinical application, the approach can be applied to mark soft tumors, serve as a pre-processing step to AI computations in generating attention maps, or support clinical decision-making by outlining regions of low diagnostic confidence. In its application alongside Python in open-source software packages like OpenCV and NumPy, the NHSS entropy-based approach is pragmatic and scalable and hence a significant resource in current radiological practice. Finally, the loop is finally completed between uncertainty theory modeling and actual application of that in medical imaging by offering an effective way to enhance precision and reliability of computer-aided diagnosis.

Application II

In the research domain of computer-assisted medical diagnosis, the article presents a new, NHSS-based method of diagnosing pneumonia from chest X-ray images and similarity calculation. The general purpose is to diagnose the infection status of suspected patients through a formal diagnostic process via image-based similarity calculation and clinical inference by algorithm (Algorithm II). Diagnosis begins with pulling chest X-ray images of the suspected pneumonia and comparing them to a reference image for pneumonia from an officially diagnosed case on a local system, which was originally retrieved from the open Kaggle data set at https://www.kaggle.com/datasets/paultimothymooney/chest-xray-pneumonia. The gray-scale images are first computed in NHSS form, with each pixel intensity being assigned to a triplet of degrees of truth, indeterminacy, and falsity primary elements of the NHSS model. Using Python, a distance and similarity algorithm is implemented to compare each suspected patient's NHSS profile with that of the confirmed pneumonia reference. The analysis yields the following NHSS profile for the patient: (0.5136, 0.9999, 0.4864), which represents the degrees of certainty (truth), uncertainty (indeterminacy), and falsity, respectively. These values are then compared against pre-defined NHSS profiles for common lung conditions such as "Normal," "Tumor," "Pneumonia," and "COVID-19," each stored as reference vectors derived from expert-labeled datasets. The similarity scores computed between the patient's profile and these conditions are as follows: Normal: 0.2525, Tumor: 0.2953, Pneumonia: 0.3368, and COVID-19: 0.3328. As the highest similarity score corresponds to Pneumonia, the system confirms this as the final diagnosis. Visualization using matplotlib allows radiologists or AI agents to overlay diagnosis results directly on the image, supporting interpretability and decision-making which can be seen in Fig. 2. This pipeline demonstrates a reliable, interpretable, and scalable method for image-based diagnosis, effectively merging fuzzy theory with advanced image processing. Future enhancements may include learning disease profiles dynamically from large medical datasets, integrating deep learning for region-based NHSS segmentation, and improving diagnostic granularity using patch-wise analysis. This fusion of NHSS and artificial intelligence marks a significant step forward in precision diagnostics and intelligent healthcare delivery.

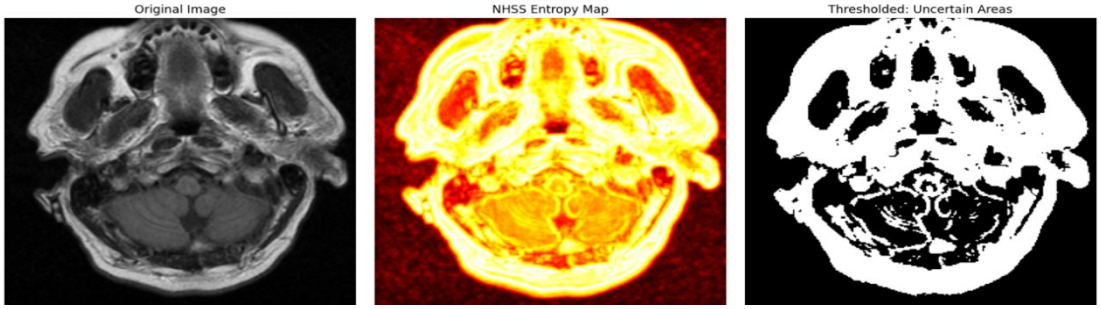

Figure 1. Uncertainty Zones Around Tumor Edges and Overlapping Tissue Intensity Areas

❖ **Algorithm 1: {NHSS Entropy-Based Medical Image Analysis}**

Require: Grayscale medical image $I \in [0,255]^{m\times n}$
Ensure: Entropy map E, Uncertainty mask M
1: Normalize the image: $I_N \leftarrow I/255.0$
2: Compute truth membership: $T \leftarrow I_N$
3: Initialize indeterminacy matrix $I_m \leftarrow 0^{m\times n}$
4: Set kernel size $k \leftarrow 5$
5: Pad I_N using reflection padding: $P \leftarrow Pad(I_N, k//2)$
6: **for** each pixel (i, j) in I_N **do**
7: Extract window: $W \leftarrow P[i : i+k, j : j+k]$
8: Compute local standard deviation: $I_m[i, j] \leftarrow std(W)$
9: **end for**
10: Normalize indeterminacy: $I_m \leftarrow I_m/max(I_m+\varepsilon)$
11: Compute falsity: $F \leftarrow 1-T$
12: Initialize entropy map: $E \leftarrow 0^{m\times n}$
13: **for** each pixel (i, j) **do**
14: $t \leftarrow T[i, j]$, $i_v \leftarrow I_m[i, j]$, $f \leftarrow F[i, j]$
15: $s \leftarrow t + i_v + f$
16: **if** $s > 1$ **then**
17: $(t, i_v, f) \leftarrow (t/s, i_v/s, f/s)$
Normalize if total exceeds 1
18: **end if**
19: Compute entropy:

$$E[i, j] \leftarrow -t \log_2(t) - i_v \log_2(i_v) - f \log_2(f)$$

20: Handle zeros by defining $x \log_2(x) = 0$ when $x = 0$
21: **end for**
22: Normalize entropy map: $E \leftarrow E/max(E)$
23: Set threshold τ (e.g., $\tau = 0.7$)
24: **for** each pixel (i, j) **do**
25: **if** $E[i, j] > \tau$ **then**
26: $M[i, j] \leftarrow 1$
27: **else**
28: $M[i, j] \leftarrow 0$
29: **end if**
30: **end for**
31: **return** E, M

❖ **Algorithm 2 : {Diagnostic NHSS Similarity Measure for Medical Image}**

1: **Input:** Medical image I, Reference NHSS Profiles $\{(T_i, I_i, F_i)\}^n i=1$
2: **Output**: Diagnosis label D
Step 1: Image Preprocessing
3: Resize I to 256×256
4: Normalize pixel values: $I \leftarrow I/255$
Step 2: Compute NHSS Triple of Input Image
5: $T \leftarrow mean(I)$
6: $I_{std} \leftarrow std(I)$
7: $I_{norm} \leftarrow I_{std}/(I_{std} + \varepsilon)$
8: $F \leftarrow 1-T$
9: $NHSS_{input} \leftarrow (T, I_{norm}, F)$

Step 3: Define Similarity Measure Function
10**: function** NHSS-SIMILARITY((T_1, I_1,F1), (T_2, I_2,F_2))
11: sim(x,y)← xy/(x+y−xy)
Avoid division by zero
12: **return** 1/3[sim(T_1,T_2)+sim(I_1, I_2)+sim(F_1,F_2)]
13: **end function**
Step 4: Compute Similarity Scores
14: **for all** diagnosis labels d_i with reference profile (T_i, I_i,F_i) **do**
15: S_i ← NHSS-SIMILARITY((T, I_{norm},F), (T_i, I_i,F_i))
16: **end for**
Step 5: Determine Diagnosis
17: D←$argmax_i$ S_i
18: **return D**

❖ **Algorithm 3: {NHSS-TOPSIS for Medical Image Diagnosis}**
1**: Input:** Medical Image I, Disease NHSS Profiles $\{(T_i, I_i,Fi)\}^n_{i=1}$, WeightsmW = [$w_T$,w_I ,w_F]
2: **Output**: Diagnosis Label D
Step 1: Image Preprocessing
3: Resize I to 256×256
4: Normalize image: I ←I/255
Step 2: Compute NHSS Triple of Patient Image
5: T_p ←mean(I)
6: I_p ←std(I)/(std(I)+ε)
7: F_p ←1−T_p
8: Patient NHSS←(T_p, Ip,Fp)
Step 3: Construct Decision Matrix
9: Let M ← matrix of size n×3 with rows (T_i, Ii,Fi) from disease profiles
Step 4: Normalize Decision Matrix
10: **for** j = 1 to 3 **do**
11: M[:, j]←M[:, j]/√($\Sigma^n_{i=1}$M[i, j]^2)
12: **end for**
Step 5: ApplyWeights
13: **for** i = 1 to n **do**
14: M[i, :]←M[i, :] ・W
15: **end for**
Step 6: Determine Ideal and Anti-Ideal Solutions
16: A+ ←max(M, axis = 0)
▷ Ideal NHSS
17: A− ←min(M, axis = 0)
▷ Anti-Ideal NHSS
Step 7: Compute Euclidean Distances
18: **for** i = 1 to n **do**
19: d^+_i ←√($\Sigma^3_{j=1}$(M[i, j]−A^+[j])^2)
20: d^-_i ←√($\Sigma^3_{j=1}$(M[i, j]−A^-[j])^2)
21: **end for**
Step 8: Calculate Closeness Coefficients
22: **for** i = 1 to n **do**
23: CCi ←d^-_i/d^-_i +d^+_i
24: **end for**
Step 9: Determine Final Diagnosis

25:D←argmax$_i$ ($CC_{i)}$
26:**return** D

❖ **Algorithm 4: {NHSS-AHP Based Diagnosis from Medical Image}**

Input: Medical image path

Output: Diagnosis label and ranking of alternatives

Procedure NHSS_AHP_Diagnosis(image_path)
1: image ← Load grayscale image from image_path
2: Resize image to 256 × 256 pixels
3:Normalize pixel values: image ← image / 255.0

Step 1: NHSS Feature Extraction

4: T ← mean(image)
5:std ← standard deviation(image)
6:I ← std / (std + ε)
7: F ← 1 − T
8:patient_nhss ← [T, I, F]

Step 2: Define Alternative Diagnoses (each as NHSS vector)

9:diagnoses ← {'Tumor':[0.85, 0.1, 0.05], 'Normal':[0.4, 0.2, 0.4], 'Inflammation':[0.6, 0.25, 0.15]}

Step 3: Construct Pairwise Comparison Matrix

10:For i = 1 to n
11: For j = 1 to n
12: If i ≠ j then
13: dist_i ← EuclideanDistance(patient_nhss, diagnoses[i])
14: dist_j ← EuclideanDistance(patient_nhss, diagnoses[j])
15: matrix[i][j] ← dist_j / dist_i
16: Else
17: matrix[i][j] ← 1
18: EndIf
19: EndFor
20: EndFor

Step 4: Compute AHP Weights

21: Compute eigenvalues and eigenvectors of matrix
22: weights ← principal eigenvector normalized

Step 5: Select Best Diagnosis

23:best_index ← argmax(weights)
24:diagnosis ← diagnoses[best_index]
25:Return diagnosis, weights

Figure 2: Final Diagnosis

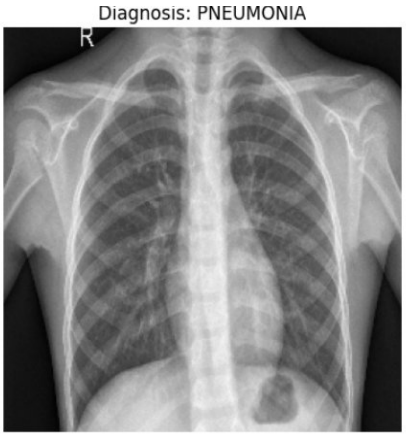

Figure 3: Final Diagnosis

Application III

This methodology introduces a structured approach for disease identification by integrating NHSS theory with the TOPSIS multi-criteria decision-making algorithm (Algorithm III). This method is designed to deal explicitly with the uncertainty, vagueness, and incomplete information often found in medical imaging. The process begins with acquiring a grayscale medical image (such as a chest X-ray), which is resized and normalized to extract meaningful pixel-level features. These pixel intensities are converted into a three-part NHSS triple representing the degrees of truth (T), indeterminacy (I), and falsity (F) thereby modeling how confidently a region in the image supports or contradicts a disease profile while accounting for uncertainty. Once the patient's NHSS triple is computed, it is compared against pre-defined NHSS profiles for several disease categories, such as "Normal," "Tumor," "Pneumonia," and "COVID-19." Each of these disease categories is modeled as a vector of (T, I, F) values based on prior clinical knowledge or expert-labeled datasets. With these profiles, a decision matrix is constructed, and TOPSIS (Technique for Order Preference by Similarity to Ideal Solution) is applied. This method first normalizes the matrix and applies weights to each criterion (e.g., 0.4 for truth, 0.3 for indeterminacy, and 0.3 for falsity). It then computes the ideal (most desirable) and anti-ideal (least desirable) solutions across all disease profiles. By calculating the Euclidean distance of the patient's NHSS triple from both the ideal and anti-ideal solutions, a closeness coefficient is derived for each disease profile. This score reflects how closely the patient's condition aligns with each diagnostic category. The disease profile with the highest closeness score is selected as the final diagnosis. In one real case application of this technique, the image analysis produced a patient NHSS triple of [0.5051, 0.9999, 0.4949], signifying moderate truth and falsity values with high indeterminacy a common scenario in medical uncertainty. When compared using the TOPSIS methodology, the closeness coefficients for various disease profiles were as follows: Normal: 0.7134, Tumor: 0.5132, Pneumonia: 0.5921, and COVID-19: 0.1671. The highest score of 0.7134 indicated the greatest similarity to the "Normal" profile, resulting in the final diagnostic decision: NORMAL, which can be seen in Fig. 3. This NHSS-TOPSIS framework offers a powerful and interpretable AI-driven diagnostic tool. It allows researchers and clinicians to evaluate medical images systematically by transforming uncertain image features into logical triplets, comparing them against established disease norms, and ranking outcomes based on their mathematical proximity to the ideal health condition. The method is flexible, scalable, and especially valuable in developing mobile health apps or AI assistants for use in low-resource clinical environments where rapid and reliable image-based diagnosis is crucial. Future extensions could incorporate deep learning models to dynamically learn disease profiles from large datasets and use region-based NHSS feature mapping to enhance diagnostic specificity.

Application IV

A medical image was analyzed using a novel diagnostic approach that combines the Neutrosophic Hypersoft Set (NHSS) framework with the Analytic Hierarchy Process (AHP) to support multi-criteria decision-making using the algorithm (Algorithm IV). The process began with image preprocessing, where the raw image was converted to grayscale, resized, and normalized to enhance consistency. From this processed image, key neutrosophic features were extracted specifically, Truth (T) representing similarity to normal tissue, Indeterminacy (I) capturing uncertainty in the image structure, and Falsity (F) denoting deviation from typical patterns. These features serve as the diagnostic fingerprint for the patient. In this case, the extracted NHSS vector was compared with reference profiles for three diagnostic alternatives: Tumor, Normal, and Inflammation, each described by expert-defined T, I, F values. A pairwise comparison matrix was constructed using neutrosophic distance, which objectively measured how close the patient's profile was to each diagnosis. This matrix replaced subjective judgment with mathematically grounded similarity assessments. By applying the eigenvector method to the matrix, priority weights for each diagnosis were calculated. The last decision was arrived at for these weights and resulted in the diagnosed prediction as Normal, ranked in the order of alternatives as: Normal (0.3939), Inflammation (0.3368), and Tumor (0.2693). Even though the result is a healthy indication, the relatively close scores reveal some diagnostic doubt shown by a high indeterminacy value for the patient's image. This procedure not only made the decision-making process more efficient but also provided a decisive reason behind every diagnosis option. The NHSS-AHP methodology facilitates integration into clinical decision-making systems as an interpretable and structured method of assessing uncertain or borderline medical cases from image data. It can assist radiologists in confirming diagnoses or referring complex cases for further evaluation.

Conclusion

This study is a valuable addition to medical diagnostics literature with three advanced AI-based methodologies developed for processing medical images and thus enhancing accuracy in infectious disease diagnosis. This combination of computational intelligence and Multi-Criteria Decision-Making (MCDM) models gives a new vision to diagnostic challenges. Utilization of four independent decision support systems including entropy-based uncertainty localization, similarity-based diagnostic assessment, AI-based TOPSIS classification, and AHP-based multi-criteria analysis presents an integrated and module-based image-based diagnostic process. All the approaches are implemented in Python and cross-validated with simulated data, supplemented with visualizations emphasizing the interpretability and usability of the findings. They not only bridge the gap between computational approaches and clinical use but also open up scopes for more efficient and responsive diagnosis. Future research will include the coupling of these AI models with wearable health sensors and real-time analytics to facilitate early disease detection and personalized treatment regimens. Furthermore, federated learning frameworks will facilitate training of models on decentralized data without jeopardizing patient data privacy. Multidisciplinary research involving machine learning, bioinformatics, clinical sciences, and public health will be critical in scaling and implementing these smart systems in actual real-world resource-constrained health settings.

Acknowledgment

This paper has received funding from the Research Council of Lithuania, project "Bridging Medical Imaging and Explainable Machine Learning: Algorithms for Precise Diagnostics", project No. S-PD-24-12.

References

1. Jayasudha, J. and Raghavi, S., 2024. Some operations on neutrosophic hypersoft matrices and their applications. Neutrosophic Systems with Applications, 21, pp.46-62.
2. X. Fei, Y. Wang, L. Dai, and M. Sui, "Deep learning-based lung medical image recognition," International Journal of Innovative Research in Computer Science and Technology, vol. 12, pp. 100-105, 2024.
3. M. Thillai, J. M. Oldham, A. Ruggiero, F. Kanavati, T. McLellan, G. Saini, et al., "Deep learning-based segmentation of CT scans predicts disease progression and mortality in IPF," American Journal of Respiratory and Critical Care Medicine, 2024.
4. J. Zheng, L. Wang, J. Gui, and A. H. Yussuf, "Study on lung CT image segmentation algorithm based on threshold-gradient combination and improved convex hull method," Scientific Reports, vol. 14, p. 17731, 2024.
5. H. T. Gayap and M. A. Akhloufi, "Deep machine learning for medical diagnosis, application to lung cancer detection: a review," BioMedInformatics, vol. 4, pp. 236-284, 2024.
6. T. Kunkyab, Z. Bahrami, H. Zhang, Z. Liu, and D. Hyde, "A deep learning-based framework (Co-ReTr) for auto-segmentation of non-small cell-lung cancer in computed tomography images," Journal of Applied Clinical Medical Physics, vol. 25, p. e14297, 2024.
7. E. K. Ruby, G. Amirthayogam, G. Sasi, T. Chitra, A. Choubey, and S. Gopalakrishnan, "Advanced Image Processing Techniques for Automated Detection of Healthy and Infected Leaves in Agricultural Systems," Mesopotamian Journal of Computer Science, vol. 2024, pp. 62-70, 2024.
8. K. Dwivedi, M. Sharkey, S. Alabed, C. P. Langlotz, A. J. Swift, and C. Bluethgen, "External validation, radiological evaluation, and development of deep learning automatic lung segmentation in contrast-enhanced chest CT," European Radiology, vol. 34, pp. 2727-2737, 2024.
9. P. Deepa, M. Arulselvi, and S. M. Sundaram, "Classification of Lung Cancer in Segmented CT Images Using Pre-Trained Deep Learning Models," International Journal of Electrical and Electronics Research, vol. 12, pp. 154-159, 2024.
10. A. S. Moosavi, A. Mahboobi, F. Arabzadeh, N. Ramezani, H. S. Moosavi, and G. Mehrpoor, "Segmentation and classification of lungs CT-scan for detecting COVID-19 abnormalities by deep learning technique: U-Net model," Journal of Family Medicine and Primary Care, vol. 13, pp. 691-698, 2024.
11. Y. Sun, J. Guo, Y. Liu, N. Wang, Y. Xu, F. Wu, et al., "METnet: A novel deep learning model predicting MET dysregulation in non-small-cell lung cancer on computed tomography images," Computers in Biology and Medicine, vol. 171, p. 108136, 2024.
12. R. Rajkumar, S. Gopalakrishnan, K. Praveena, M. Venkatesan, K. Ramamoorthy, and J. J. Hephzipah, "DARKNET-53 Convolutional Neural Network-Based Image Processing for Breast Cancer Detection," Mesopotamian Journal of Artificial Intelligence in Healthcare, vol. 2024, pp. 59-68, 2024.
13. J. Jiang and H. Veeraraghavan, "Self-supervised pretraining in the wild imparts image acquisition robustness to medical image transformers: an application to lung cancer segmentation," in Medical Imaging with Deep Learning, 2024.
14. X. Chen, R. P. Mumme, K. L. Corrigan, Y. Mukai-Sasaki, E. Koutroumpakis, N. L. Palaskas, et al., "Deep learning–based automatic segmentation of cardiac substructures for lung cancers," Radiotherapy and Oncology, vol. 191, p. 110061, 2024.
15. S. H. Hosseini, R. Monsefi, and S. Shadroo, "Deep learning applications for lung cancer diagnosis: a systematic review," Multimedia Tools and Applications, vol. 83, pp. 14305-14335, 2024.
16. W. Ding, H. Wang, J. Huang, H. Ju, Y. Geng, C.-T. Lin, et al., "FTransCNN: Fusing Transformer and a CNN based on fuzzy logic for uncertain medical image segmentation," Information Fusion, vol. 99, p. 101880, 2023.

17. C. Kaushal, M. K. Islam, S. A. Althubiti, F. Alenezi, and R. F. Mansour, "A framework for interactive medical image segmentation using optimized swarm intelligence with convolutional neural networks," Computational intelligence and neuroscience, vol. 2022, p. 7935346, 2022.
18. V. Narayan, M. Faiz, P. K. Mall, and S. Srivastava, "A comprehensive review of various approach for medical image segmentation and disease prediction," Wireless Personal Communications, vol. 132, pp. 1819-1848, 2023.
19. C.-L. Chin, J.-C. Lin, C.-Y. Li, T.-Y. Sun, T. Chen, Y.-M. Lai, et al., "A novel fuzzy dbnet for medical image segmentation," Electronics, vol. 12, p. 2658, 2023.
20. Q. Shi, S. Yin, K. Wang, L. Teng, and H. Li, "Multichannel convolutional neural network-based fuzzy active contour model for medical image segmentation," Evolving Systems, vol. 13, pp. 535-549, 2022.
21. N. Nagaraja Kumar, T. Jayachandra Prasad, and K. S. Prasad, "An intelligent multimodal medical image fusion model based on improved fast discrete curvelet transform and type-2 fuzzy entropy," International Journal of Fuzzy Systems, vol. 25, pp. 96-117, 2023.
22. M. Ahammed, M. Al Mamun, and M. S. Uddin, "A machine learning approach for skin disease detection and classification using image segmentation," Healthcare Analytics, vol. 2, p. 100122, 2022.
23. A. Talamantes-Roman, G. Ramirez-Alonso, F. Gaxiola, O. Prieto-Ordaz, and D. R. Lopez-Flores, "A TransUNet model with an adaptive fuzzy focal loss for medical image segmentation," Soft Computing, pp. 1-17, 2024.
24. H. Hooda and O. P. Verma, "Fuzzy clustering using gravitational search algorithm for brain image segmentation," Multimedia Tools and Applications, vol. 81, pp. 29633-29652, 2022.
25. C. Wang, X. Lv, M. Shao, Y. Qian, and Y. Zhang, "A novel fuzzy hierarchical fusion attention convolution neural network for medical image super-resolution reconstruction," Information Sciences, vol. 622, pp. 424-436, 2023.